Materials Research. 2023; 26:e20220329
DOI: https://doi.org/10.1590/1980-5373-MR-2022-0329

Hydroxylation Studies on High-Solid Load Magnesia Aqueous Suspensions

***Rafael Salomão*[a]*, *Leandro Fernandes*[a]

[a]*Universidade de São Paulo, Escola de Engenharia de São Carlos, Departamento de Engenharia de Materiais, São Carlos, SP, Brasil.*

Received: July 21, 2022; Revised: September 27, 2022; Accepted: November 05, 2022

The magnesia (MgO) hydroxylation behavior in dilute suspensions (below 50% volumetric solid loads) has been extensively studied over the past decades due to its role in refractory castables. However, its equivalent effects on concentrated systems have not been analyzed in such a systemic way, although they are known to be as or more deleterious than those observed in dilute systems. This study focuses on the hydroxylation behavior of different sources of magnesia (sinter and caustic magnesia) in aqueous suspensions prepared at various solids concentrations (17-96 vol%) and shaped by distinct methods. They were analyzed by thermogravimetry, apparent volumetric expansion measurements, X-ray diffraction, scanning electron microscopy, and *in situ* temperature measurements during curing. The ratio between experimental and theoretical extents of the hydroxylation degree resulted in the reaction yield. A comparison between samples containing the same water amount revealed those with caustic magnesia showed a faster evolution of hydroxylation degree, apparent volumetric expansion, and higher maximum internal temperature during curing. In both systems, the yield levels of compositions of heavier solid loads were higher, despite the small quantity of hydroxylation products formed. Significant differences in the products' microstructure were observed and related to the ions' mobility toward crystallization nuclei.

Keywords: *Magnesia, hydroxylation, sinter, caustic, expansion, solid load.*

1. Introduction

Magnesium oxide (MgO), or magnesia, is a key raw material for steelmaking due to its high refractoriness (above 2800ºC melting point) and resistance to molten slag corrosion[1-5]. Nevertheless, the deleterious effects on the reactions of magnesia in contact with water, i.e., its expansive hydroxylation behavior, are equally important and well-documented[6-12].

In suspensions prepared with high-purity water (e.g., mostly free of dissolved $(CO_3)^{2-}$ ions), the hydroxylation of MgO particles begins with the protonation of their external surfaces and the alkalinization of water (Equation 1)[13-21]:

$$MgO + H\ O \rightarrow MgOH^+ + OH^- \quad (1)$$

$MgOH^+$ ions then dissolve in water up to the point of saturation, significantly increasing both medium's ionic conductivity and strength[22-25]. Such a condition is known as the induction period[26,27] and can last from a few seconds to up to several hours[7], depending on the MgO source[26,28], its physical properties[29,30], and test conditions[29,31,32]. The saturated solution then begins to form magnesium hydroxide ($Mg(OH)_2$) or brucite[33-39], whose particles precipitate (Equation 2) at unreacted MgO surfaces.

$$MgOH^+ + OH^- \rightarrow Mg(OH)_2 \quad (2)$$

Because density values of MgO (3.5 $g.cm^{-3}$) and $Mg(OH)_2$ (2.4 $g.cm^{-3}$) are significantly different[1,5,6,29,40], the hydroxylation-precipitation process generates compressive forces at particles' surfaces, resulting in their breakage[16,17,28,29,41]. The exposure of unreacted material restarts the process and increases the hydroxylation rate[29,39,41,42]. In macroscopic structures, such forces produce significant volumetric expansion that usually ends up cracking and crumbling the material[1,2,6,8,10,11,43-46]. Several solutions have been designed towards preventing such damages by hampering MgO hydroxylation[2,7,12,32,45], changing the morphology of its products[10,30-32,43,46,47], or generating a surrounding microstructure for accommodating the extra volume produced[6,8,9,43,44,48].

Previous studies on the impact of intrinsic variables on MgO hydroxylation have reported a significant temperature increase during the process[2,26,28,29], which is related to the excess of energy contained in the dissolved $MgOH^+$ ion released as heat after the precipitation of $Mg(OH)_2$ particles[17,33]. In some cases, such an effect accelerates the reaction and is more intense at high curing temperatures and in samples of larger volume[29]. Other reports have suggested MgO suspensions prepared with distinct solid loads may display different hydroxylation behaviors[28]. In such systems, the balance between MgO being dissolved and the precipitation of $Mg(OH)_2$ may be affected by the large quantity of water to be heated in the spaces amongst solid particles. Although such aspects were deeply studied in dilute aqueous suspensions, such as refractory castables (10-50 vol% of solids for self-flow[1,3,4] and 50-80 vol% for vibrate ones[49,50]), they remain unexplored for more concentrated systems such as refractory mortars (80-95 vol% of solids)[6,8,12] and pressed pellets and

*e-mail: rsalomao@sc.usp.br

bricks (above 95 vol% of solids)[1,2]. Even though these classes of pre-shaped refractories contain little or no water in their original formulations, hydroxylation reactions can occur due to contact with atmospheric moisture[14,15], hydraulic cementing agents[9,10], or layers of spray-applied refractory concrete for maintenance repair[1,2]. Because such situations are frequent in steelmaking industries and their potential mechanical damage can lead to long equipment idle time, the study of MgO hydroxylation in highly concentrated suspensions can have a significant technological impact.

The present study analyzed the hydroxylation behavior of two sources of magnesia, namely magnesia sinter (or hard-burnt magnesia) and caustic magnesia (or dead-burnt magnesia) of similar chemical composition and average diameter in aqueous suspensions prepared at various solids concentrations (from 17 vol% up to 96 vol%). MS is typically obtained by sintering pellets of magnesium hydroxide ($Mg(OH)_2$) or carbonate ($MgCO_3$) at temperatures as high as 1800ºC, which generate very dense structures with large and well-built crystals and practically no significant surface contamination by $(CO_3)^{2-}$ and $(OH)^-$ ions (Figure 1a)[1,2,5]. After milling and sieving, the particles attained show a low specific surface area and practically contain no internal grain boundaries[28]. Consequently, their chemical reactivity and hydroxylation rate are low under testing temperatures below 100ºC. On the other hand, CM is attained as a by-product of sinter production at sleeve filters that retain fines at furnaces' overflow[5]. Because of the lower temperatures involved (700-1000ºC), the crystalline structure of the MgO attained after the $MgCO_3$ decarbonation remains highly defective and its particles show a much higher specific surface area and reactivity due to the large fraction of mesopores and numerous cracks formed during gas evolution (Figure 1b)[23,27,28,40].

Such raw materials were selected because they also largely differ in their ability to form castable self-flow suspensions or thick pastes that require pressing to be shaped[28,29]. Their hydroxylation behaviors were investigated by thermogravimetric analysis (TGA), X-ray diffraction (XRD), scanning electron microscopy (SEM), and *in situ* temperature measurements during curing tests. Concomitantly, the volumetric expansion that follows such reactions was evaluated by apparent volumetric expansion (AVE) measurements[6,7,28,29,50].

2. Materials and Methods

As-received particles of magnesia sinter (MS, High-Purity M30, RHI-Magnesita, Brazil, Figure 1a) and caustic magnesia (CM, Q-MAG AR200, RHI-Magnesita, Brazil, Figure 1b) were initially characterized regarding their composition (X-ray dispersive spectroscopy, Shimadzu, EDX 720, Japan, after calcination at 1000ºC for 5 h), particles' diameter distribution (acoustic emission method, DT-1202, Dispersion Technology Inc., USA), reactivity with water (neutralization of acetic acid solution method, ASTM C544 – 03, 2013, "Standard Test Method for Hydration of Dead Burned Magnesite or Periclase Grain"), solid density (Helium pycnometry, Ultrapyc 1200e, Quantachrome Instruments, USA), specific surface area (high-purity nitrogen adsorption, BET method, Nova

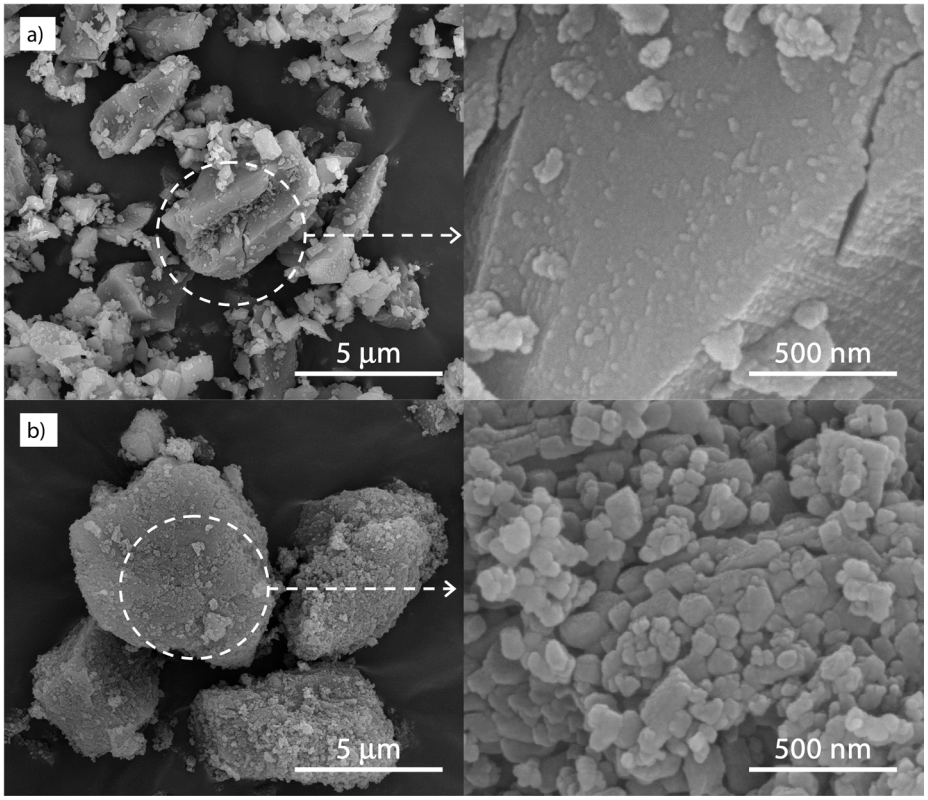

Figure 1. Microstructure of as-received a) magnesia sinter (MS) and b) caustic magnesia (CM) particles employed in this study.

1200e, Quantachrome Instruments, USA, ASTM C 1069-09 standard "Standard Test Method for Specific Surface Area of Alumina or Quartz by Nitrogen Adsorption"), and moisture and water content (Thermogravimetric analysis, TGA-Q50, TA Instruments, 25-1000ºC, synthetic air atmosphere) (Table 1).

Mixtures of MS or CM and twice-distilled water (ionic conductivity of 0.07 μS/cm, at 25 ± 0.5ºC) were prepared with different solid loads and shaped by uniaxial pressing or direct casting (Table 1). To prepare pressed samples, water was slowly sprayed by a peristaltic pump (Masterflex, LS77201-60, USA), working under 0.01 $cm^3.s^{-1}$ constant flow, and connected to an ultrasonic nozzle, inside a closed-vessel propeller blender (operating at 500 rpm for 5 min) containing magnesia particles. After mixing, wet particles were sieved (D_{Part} < 100 μm) to ensure optimum homogenization of the mixture, and uniaxially pressed (40 MPa, 60 s) as 40 mm diameter per 40 mm height cylinders. For the directly cast samples, magnesia particles and water were mixed in a paddle mixer (PowerVisc, Ika, Germany) at 1000 rpm for 5 minutes. The suspensions attained were cast in thin non-adherent polymeric molds (Figure 2a; pressed samples were placed in similar molds after extraction and demolding).

After the samples had been shaped or cast, a thin K-type thermocouple was inserted at their centers and half-heights for monitoring the inner temperature during hydroxylation tests (Figure 2b)[7,28,29]. They remained in sealed flasks in an environment of close to 100% relative humidity and

Table 1. Characteristics of the magnesia sources and compositions tested.

Particles' characteristics		Sources of magnesia	
		[a] *Magnesia sinter (MS)*	[b] *Caustic magnesia (CM)*
Composition (wt%)	MgO	98.3	98.4
	CaO	0.72	0.71
	SiO_2	0.18	0.15
	Al_2O_3	0.18	0.03
	Fe_2O_3	0.21	0.32
	Na_2O	0.16	0.29
	MnO	0.25	0.10
Particle size (μm, D_{50}/D_{90})		8 / 29	12 / 48
Activity (s)		2512	50
Solid density (ρ, $g.cm^{-3}$)		3.47	3.49
[c] Relative density ($\rho/\rho_{Theoretical}$, %)		98.7	99.4
Specific surface area (SSA, $m^2.g^{-1}$)		1.5	23
Humidity (wt%, 2 h at 200ºC)		0.8	1.2
Loss of ignition(wt%, 200-1000ºC)		0.1	0.3
Compositions tested		Magnesia sinter (MS)	Caustic magnesia (CM)
MgO (mol%/wt%/vol%)	Water (mol%/wt%/vol%)	*Processing method*	*Processing method*
97.56 / 98.89 / 96.19	2.44 / 1.11 / 3.81	Uniaxial pressing (Maximum solid load to press)	-
95.24 / 97.81 / 92.67	4.76 / 2.19 / 7.33	Uniaxial pressing	-
90.91 / 95.72 / 86.34	9.09 / 4.28 / 13.66	Uniaxial pressing	Uniaxial pressing (Maximum solid load to press)
83.33 / 91.79 / 75.96	16.67 / 8.21 / 24.04	Uniaxial pressing	Uniaxial pressing
76.92 / 88.18 / 67.81	23.08 / 11.82 / 32.19	Cast under vibration (Maximum solid load to form a uniform suspension)	Uniaxial pressing
71.43 / 84.83 / 61.24	28.57 / 15.17 / 38.76	Cast under vibration	Uniaxial pressing
66.67 / 81.73 / 55.83	33.33 / 18.27 / 44.17	Cast, self-flow	Uniaxial pressing
57.14 / 74.89 / 45.73	42.89 / 25.11 / 54.27	Cast, self-flow	Cast under vibration (Maximum solid load to form a uniform suspension)
50.00 / 69.11 / 38.73	50.00 / 30.89 / 61.27	Cast, self-flow (Stoichiometric MgO/water ratio)	Cast, self-flow (Stoichiometric MgO/water ratio)
40.00 / 59.86 / 29.64	60.00 / 40.14 / 70.36	Cast, self-flow	Cast, self-flow
33.33 / 52.80 / 24.01	66.67 / 47.20 / 75.99	Cast, self-flow	Cast, self-flow
25.00 / 42.72 / 17.40	75.00 / 57.28 / 82.60	Cast, self-flow	Cast, self-flow

a) High purity M30 (RHI-Magnesita, Brazil); b) Q-MAG AR200 (RHI-Magnesita, Brazil); c) $\rho_{Theoretical}$ = 3.51 $g.cm^{-3}$

60ºC ± 0.5ºC for up to 168 h[6,50]. During that period, their external dimensions (height, H_i, and diameter, D_i, in mm) were measured every 24 h (Figure 2c-d and their external volume (V_i) and apparent volumetric expansion (AVE, %) were calculated by Equations 3 and 4, where lower indices 0 and E indicate, respectively, the initial condition and the condition after a certain hydroxylation period and t is the thickness of each mold (in mm).

$$V_i = \frac{H_i \times \pi \times (D_i - 2 \times t)^2}{4} \quad (3)$$

$$AVE = 100\% \times \left[\frac{V_E - V_0}{V_0} \right] \quad (4)$$

The AVE parameter indicates the level of damage caused by hydroxylation expansion to ceramic structure and a close relationship with hydroxylation degree ($W_{H\,Exp}$, described ahead) and loss of mechanical strength and rigidity. AVE's most important characteristic is it is continuously measured for the same sample at any time interval required. A detailed explanation of such a technique and its uses can be found elsewhere[6,50].

Equivalent samples were removed from hydroxylation tests every 24 h, crushed, sieved (D_{Part} < 100 µm), and dried overnight at 120ºC under vacuum for the removal of unreacted water. After weighting (M_H, g), they were calcined at 1000ºC for 5 h to fully dehydroxylate $Mg(OH)_2$ and weighed again (M_C, g). Equation 5 provided, respectively, experimental ($W_{H\,Exp}$) and maximum theoretical ($W_{H\,Theor}$) values of hydroxylation degree (W_H, wt%) attained for each combination of magnesia source and water. The 0.447 therm is a numerical adjustment, based on the molar mass values of MgO (40.303 g.mol^{-1}) and $Mg(OH)_2$ (58.318 g.mol^{-1}), for making W_H vary from 0, when there is no reaction, up to 100%, for stoichiometric hydroxylation reactions[1,7,28,29,40].

$$W_{H\,Exp} or\ W_{H\,Theor} = 100\% \times [(M_H - M_C) / (0.447 \times M_C)] \quad (5)$$

$W_{H\,Exp}$ indicates the extension of the hydroxylation reaction, whereas the $W_{H\,Theor}$ represents the maximum hydroxylation degree to be attained if the reaction occurs stoichiometrically for each particular formulation. As an example, in a system containing 1 mol of MgO and 0.5 mol of water, the maximum theoretical hydroxylation degree that can be attained is 50%

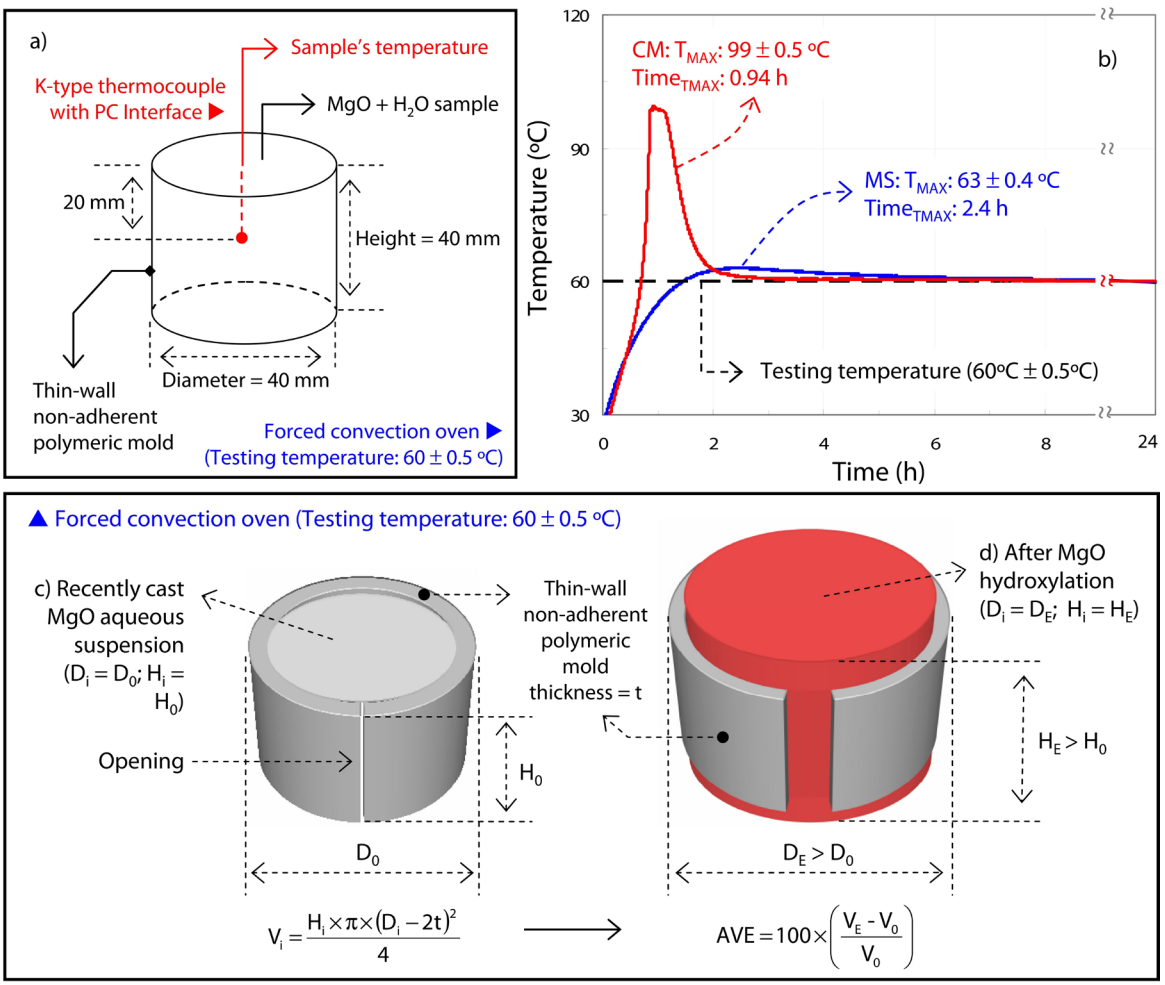

Figure 2. Schematic representation of a) samples employed for hydroxylation tests with details on b) inner temperature monitoring and analysis during the curing period and c) molds for apparent volumetric expansion (AVE) measurements.

because there is not enough water to fully consume MgO. Experimentally, on the other hand, hydroxylation degree levels lower than 50% can be observed for the same system during the first hours of testing, for low-reactivity MgO sources and low-temperature testing conditions. Therefore, the $W_{H\,Exp}$ / $W_{H\,Theor}$ ratio (ranging from 0 up to 100%) can be adopted for the evaluation of the reaction yield.

The products of hydroxylation tests were identified by X-ray diffraction (XRD, Rotaflex RV 200B, Rigaku-Denki Corp., Japan; with Kα = Cu radiation, λ = 0.15406 nm, in the 2θ range from 10º to 80º at a 1º.min^{-1} scan rate) and quantified by Rietveld method (MATCH! software, 3.8 version, Germany) and by thermogravimetry (TGA-Q50, TA Instruments, 25-1000ºC, synthetic air atmosphere, 5ºC. min^{-1} heating rate). Their microstructure was observed by field emission scanning electron microscopy (FEG-SEM, FEI 7500F, Holland).

3. Results and Discussion

Caustic magnesia (CM) and magnesia sinter (MS) exhibited significantly different hydroxylation behaviors for the same testing time in all concentrations tested. In general, CM-containing samples showed a faster evolution of hydroxylation degree ($W_{H\,Exp}$), apparent volumetric expansion (AVE) (Figure 3), and more intense heating (T_{Max}) above testing temperature (Figure 4) in comparison to MS-containing ones. Previous studies have reported similar results, explained through the microstructure of the MgO particles[28,29,40], as discussed in the first section.

Regarding the yield of hydroxylation reactions (Figure 5), all CM-containing samples showed $W_{Exp}/W_{H\,Theor}$ ratios above 94%, indicating the reactions consumed practically all water or all MgO available towards forming $Mg(OH)_2$. On the other hand, only concentrated suspensions (81-99 vol% of MgO) provided an above 90% yield for the MS-containing samples. The understanding of such differences requires analyses of MgO hydroxylation as a two-sequential-step mechanism, i.e., dissolution of MgO and precipitation of $Mg(OH)_2$[20-23,26]. After the initial stages of hydroxylation, the precipitation of $Mg(OH)_2$ particles tends to block the unreacted MgO surfaces reducing their dissolution rate, hence the overall speed of the process[20,21,23]. Such behavior occurs more intensely in diluted suspensions due to the large space for accommodating the hydroxylation products. In high solid load suspensions, on the other hand, the water available is located mainly at the particles' surface rather than in the empty spaces amongst them. Consequently, the dissolution step can occur with no kinetic barriers imposed by precipitated products[31,42]. After all water in the mixture has been consumed, the reaction stops, and a high yield is attained despite the small amount of $Mg(OH)_2$ produced.

Another important aspect of the results is the maximum temperature achieved by the samples during the tests (Figure 4).

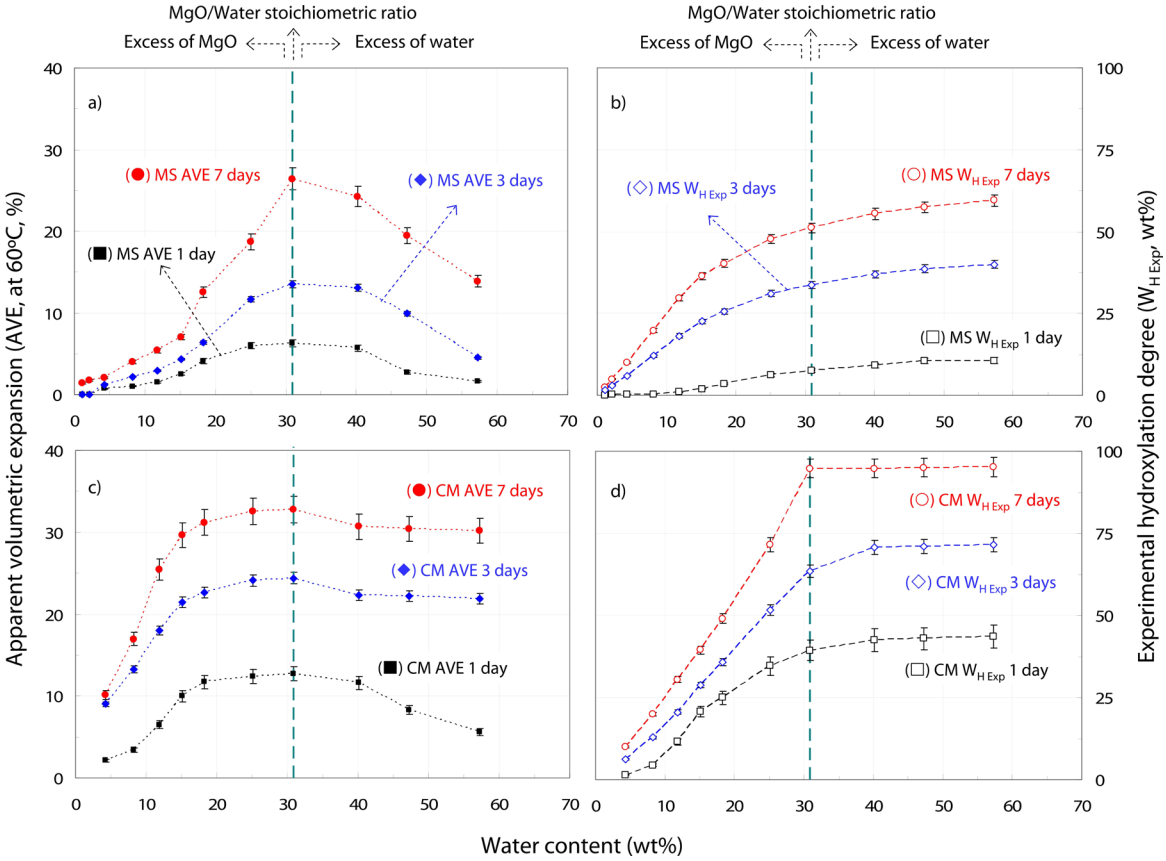

Figure 3. Evolution of apparent volumetric expansion (AVE) and experimental hydroxylation degree ($W_{H\,Exp}$) for samples prepared with different contents of a-b) magnesia sinter (MS) and c-d) caustic magnesia (CM) during hydroxylation tests (up to 7 days at 60ºC).

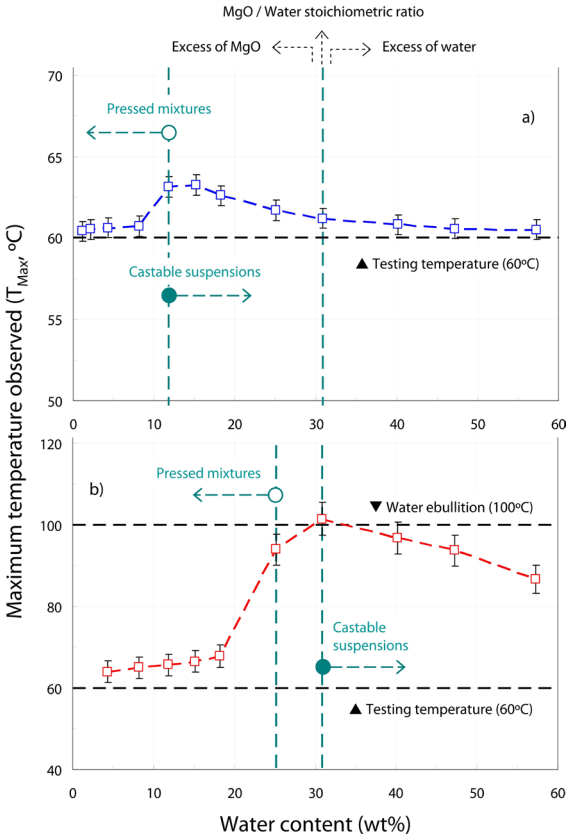

Figure 4. Combined effects of varying solid load and shaping process on the maximum temperature observed during hydroxylation tests for samples prepared with a) magnesia sinter, MS, or b) caustic magnesia, CM (after 7 days at 60ºC).

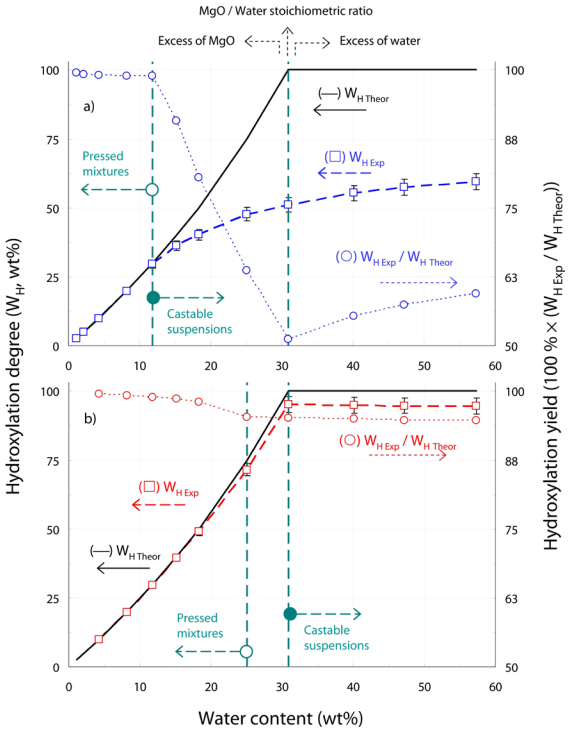

Figure 5. Combined effects of varying solid load and shaping process on hydroxylation degree and yield during hydroxylation tests for samples prepared with a) magnesia sinter, MS, or b) caustic magnesia, CM, (after 7 days at 60ºC).

Whereas, the maximum temperature for MS-containing samples was 5ºC above the testing one, over 40ºC increases were observed for CM-containing samples, particularly for castable suspensions. Such an exothermic event is related to the excess of free energy contained in the dissolved $MgOH^+$ ions during the saturation period and which is released after the precipitation of $Mg(OH)_2$ particles[7,26,33]. Because CM intense dissolution takes place at the first moments of contact with water, saturation and precipitation steps also occur in a short time[26,2829]. Since the heat evolution rate is faster than its withdrawal from the system, the samples' inner temperature rises and increases the speed of the whole reaction in a self-catalytic process. Interestingly, for both systems, samples of high (MS: 1.1-8.2 wt%; CM: 4.3-18.3wt%) or low (MS: 40.1-57.3 wt%; CM: 57.3 wt%) MgO content showed less intense temperature increases than the stoichiometric composition. In the first case, the short extension of the MgO hydroxylation reaction released small energy content, whereas, in the latter, the excess water consumed a significant part of the energy to be heated a few degrees above the testing temperature.

After the hydroxylation tests and drying, all compositions resulted in mixtures of different proportions of unreacted MgO (periclase) and $Mg(OH)_2$ (brucite) (Figure 6). No traces of $MgCO_3$ (magnesite), $(Mg_5(CO_3)_4(OH)_2.4H_2O)$ (hydromagnesite), or other compounds were detected under those testing conditions. Previous reports indicate that small traces of carbonated compounds are expected to be found at MgO's particles surfaces due to the contact with dissolved $(CO_3)^{2-}$ ions[51-54]. Under the tested conditions, however, carbonation reactions are not favored due to the low concentration of $(CO_3)^{2-}$ ions dissolved in twice-distilled water at 60ºC[55,56].

According to strong linear trends between the experimental hydroxylation degree ($W_{H\ Exp}$) and the mass ratio between crystalline phases present (MgO and $Mg(OH)_2$, determined by the Rietveld method) (Figure 7), the higher the $W_{H\ Exp}$ values, the smaller the quantity of unreacted MgO after the hydroxylation test. Nevertheless, the morphology of precipitated $Mg(OH)_2$ particles varied significantly in the function of the MgO source and solid load in the suspensions (Figure 8). For MS-containing samples prepared with small amounts of water (Figures 8a-b), $Mg(OH)_2$ precipitation occurs initially over MS surfaces due to its very low solubility[20,22,31]. The tensile efforts from the density mismatch between the materials led to the exposure of unreacted MgO surfaces as elongated rods of triangular cross-sections[28]. The $Mg(OH)_2$ particles formed detached and remained as thin irregular clusters amongst the prismatic rods. Regarding suspensions prepared with higher water content (Figures 8c-d), ions showed greater mobility during the tests, and more hydroxylation products were formed. Therefore, the microstructure of hydroxylation products consists of large plate-like hexagonal crystals of

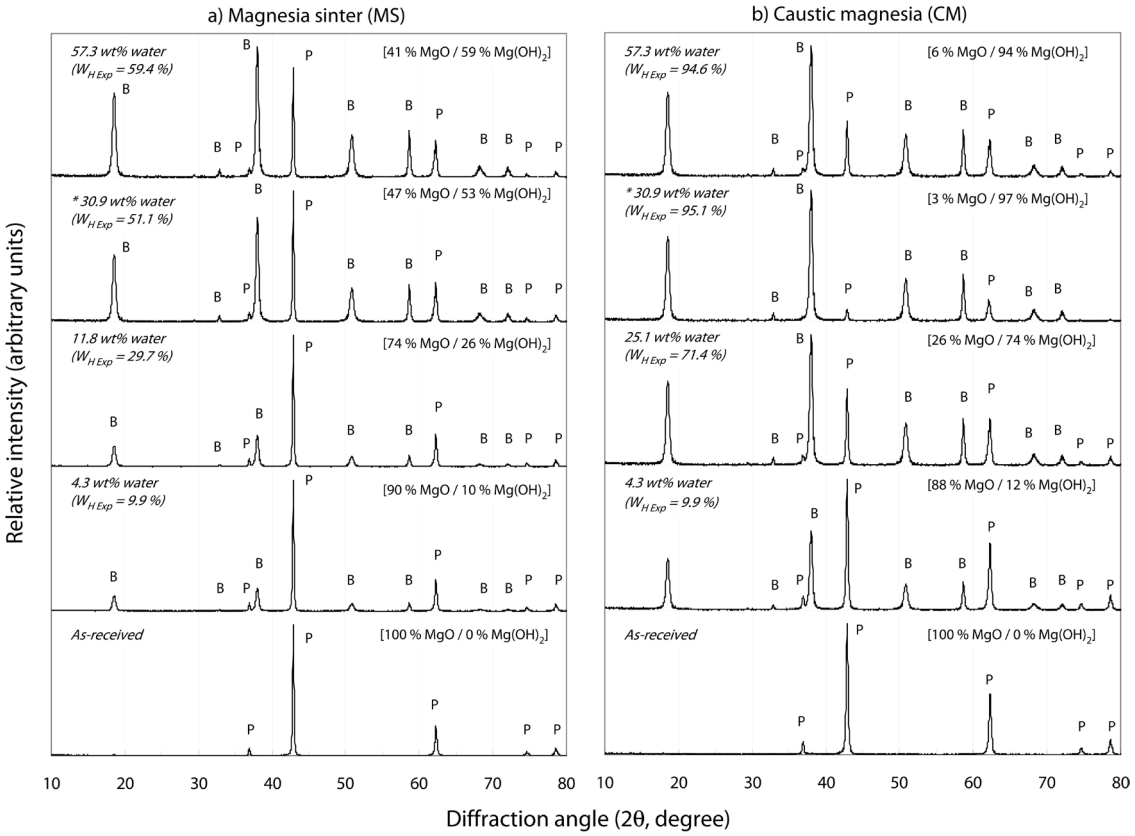

Figure 6. X-ray diffraction patterns for samples prepared with different contents of a) magnesia sinter (MS) and b) caustic magnesia (CM) after hydroxylation tests (7 days at 60ºC). The experimental hydroxylation degree ($W_{H\,Exp}$, wt) and the mass ratio between the crystalline phases identified (in square brackets) are shown for each composition. List of symbols: P = Periclase (α-MgO, PDF 1-1234); B = Brucite (α-$Mg(OH)_2$, PDF 1-1169).

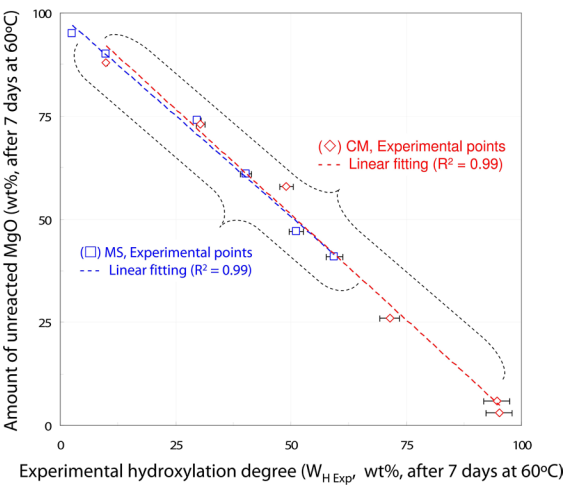

Figure 7. Relationship between the amount of unreacted MgO (quantified from XRD results, Figure 6) and experimental hydroxylation degree observed after hydroxylation tests ($W_{H\,Exp}$, Figure 3, after 7 days at 60ºC).

$Mg(OH)_2$ grown over each other and that cover a significant fraction of unreacted and fractured MS particles.

On the other hand, CM suspensions produced hexagonal plate-like particles of $Mg(OH)_2$ whose average diameter and shape regularity increased from concentrated suspensions (Figures 8e-f) to more diluted ones (Figures 8g-h). Such an effect is typically observed in particles attained from controlled precipitation of dissolved ions[33,34,37,40]. In those processes and for concentrated solutions, nucleation is the main free-energy-lowering mechanism, leading to a rapid formation of clusters of thin particles. Oppositely, diluted ion solutions display a lower driving force for nucleation and, consequently, each crystallization nucleus grows intensively and shows regular geometry, following a most stable habit. Similar to the behavior of MS suspensions, the higher the water content, the larger the $Mg(OH)_2$ particles formed and the more regular their geometry.

From a technological point of view, the results somehow explain why MgO hydroxylation produces such different effects in the function of the ceramic structure tested[1,2,5]. For sintered MS bricks, for instance, a small quantity of water from air humidity can produce high-yield hydroxylation reactions at exposed surfaces, resulting in severe cracks and dusting, even if a small portion of $Mg(OH)_2$ has been formed[1]. On the other hand, a large amount of water in MgO-containing self-flowing castables prevents the effects of heat release and the spaces amongst particles are wide enough to accommodate hydroxylation products[50]. Therefore, even if a significantly larger quantity of $Mg(OH)_2$ is formed, its macroscopic effects (e.g., AVE and cracks) are less intense than those on bricks.

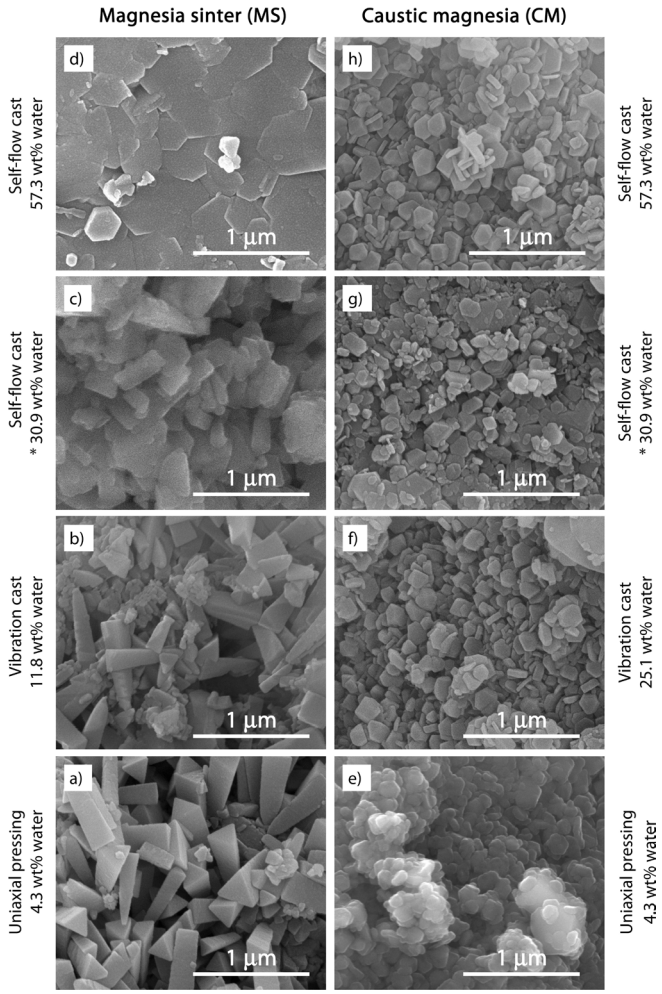

Figure 8. Combined effects of varying solid load and shaping process on magnesia sinter (MS) or caustic magnesia (CM) particles' microstructures attained after hydroxylation tests (after 7 days at 60ºC).

Nevertheless, CM can be used in applications that require its full hydroxylation even under low availability of water such as soil corrector[5,26].

4. Conclusions

The MgO sources (caustic magnesia, CM, or magnesia sinter, MS) exhibited distinct hydroxylation behaviors when tested as aqueous suspensions of different solid loads shaped by uniaxial pressing or direct casting. In general, the high chemical reactivity of caustic magnesia particles resulted in hydroxylation reactions of higher-yielding and greater apparent volumetric expansion (AVE) in comparison to equivalent suspensions containing MgO sinter.

For the same source of MgO, those compositions with higher solid content showed hydroxylation reactions with higher yields despite the lower total amount of $Mg(OH)_2$ formed and the lower levels of AVE observed. Such suspensions exhibited a self-catalytic behavior according to which hydroxylation reactions occurred directly at the surfaces of MgO particles, exposing unreacted material and promoting significantly higher heat evolution. On the other hand, in diluted compositions, the precipitation of $Mg(OH)_2$ at the surfaces of unreacted MgO particles reduced their dissolution-precipitation and heat evolution rates, hence the overall reaction speed and yield.

Although all hydroxylation tests resulted in mixtures of different proportions of MgO and $Mg(OH)_2$ after drying, the microstructure of their products significantly differed. Diluted castable suspensions of CM produced $Mg(OH)_2$ particles of the highest regularity in size and shape with a small amount of unreacted MgO, whereas pressed MS led to compacts of fragmented MgO particles surrounded by $Mg(OH)_2$ clusters.

5. Acknowledgments

The authors acknowledge Brazilian Research Foundations FAPESP (2010-19274-5; 2017/06738-2; 2018/19773-3), CNPq (305877/2017-8; 304081/2020-5), and CAPES (Finance Code 001) for supporting this research, and Magnesita-RHI (Brazil) for the samples of magnesia sinter and caustic magnesia. They are also indebted to the Electron Microscopy Laboratory of Advanced Materials Research Support Center (SMM/IFSC) for the SEM images.

6. References

1. Kitamura A, Onizuka K, Tanaka K. Hydration characteristics of magnesia. Taikabutsu Overs. 1995;16(3):3-11.
2. Kaneyasu A, Yamamoto S, Yoshida A. Magnesia raw materials with improved hydration resistance. Taikabutsu Overs. 1996;17(2):21-6.
3. Innocentini MDM, Salomão R, Ribeiro C, Cardoso FA, Pandolfelli VC, Rettore RP, et al. Permeability of fiber-containing refractory castables. Am Ceram Soc Bull. 2002;81(8):65-8.
4. Innocentini MDM, Ribeiro C, Salomão R, Pandolfelli VC, Bittencourt LRM. Assessment of mass loss and permeability changes during the dewatering process of refractory castables containing polypropylene fibers. J Am Ceram Soc. 2002;85(8):2110-2. http://dx.doi.org/10.1111/j.1151-2916.2002.tb00413.x.
5. Shand MA. The Chemistry and technology of magnesia. New Jersey: John Wiley & Sons; 2006.
6. Salomão R, Pandolfelli VC. Magnesia sinter hydration-dehydration behavior in refractory castables. Ceram Int. 2008;34(8):1829-34. http://dx.doi.org/10.1016/j.ceramint.2007.06.009.
7. Amaral LF, Oliveira IR, Salomão R, Frollini E, Pandolfelli VC. Temperature and common-ion effect on magnesium oxide (MgO) hydration. Ceram Int. 2010;36(3):1047-54. http://dx.doi.org/10.1016/j.ceramint.2009.12.009.
8. Souza TM, Braulio MAL, Luz AP, Bonadia P, Pandolfelli VC. Systemic analysis of MgO hydration effects on alumina-magnesia refractory castables. Ceram Int. 2012;38(5):3969-76. http://dx.doi.org/10.1016/j.ceramint.2012.01.051.
9. Cao F, Miao M, Yan P. Hydration characteristics and expansive mechanism of MgO expansive agents. Constr Build Mater. 2018;183(20):234-42. http://dx.doi.org/10.1016/j.conbuildmat.2018.06.164.
10. Mo L, Fang J, Hou W, Ji X, Yang J, Fan T, et al. Synergetic effects of curing temperature and hydration reactivity of MgO expansive agents on their hydration and expansion behaviours in cement pastes. Constr Build Mater. 2019;207(20):206-17. http://dx.doi.org/10.1016/j.conbuildmat.2019.02.150.
11. Cao F, Yan P. The influence of the hydration procedure of MgO expansive agent on the expansive behavior of shrinkage-compensating mortar. Constr Build Mater. 2019;202(30):162-8. http://dx.doi.org/10.1016/j.conbuildmat.2019.01.016.
12. Fini DS, Miguel VC, Pinto VS, Pandolfelli VC, Moreira MH, Luz AP. Aluminum lactate role in improving hydration and drying behavior of MgO-bonded refractory castables. Ceram Int. 2020;46(10):17093-102. http://dx.doi.org/10.1016/j.ceramint.2020.04.006.
13. Hüttig GF. Die kinetic der alterung von aktivem magnseiumoxyd. Kolloid-Zeitschrift. 1951;124(3):160-3.
14. Finch GI, Sinha KP. On reaction in the solid state. Proc R Soc Lond A. 1957;239:145-53.
15. Razouk RI, Mikhail RS. The hydration of magnesium oxide from vapor phase. J Phys Chem. 1958;62:920-5.
16. Glasson DR. Reactivity of lime and related oxides: hydration of magnesium oxide. J Appl Chem (Lond). 1963;13(3):119-23. http://dx.doi.org/10.1111/j.1151-2916.1963.tb14602.x.
17. Layden GK, Brindley GW. Kinetics of vapor-phase hydration of magnesium oxide. J Am Ceram Soc. 1963;46(11):518-22.
18. Anderson PJ, Horlock RF, Oliver JF. Interaction of water with the magnesium oxide surface. Trans Faraday Soc. 1965;61(516):2754-62.
19. Feitknecht W, Braum H. Der Mechanismus der hydratation von magnesiumoxid mit wasserdampf. Helv Chim Acta. 1967;50(7):2040-53.
20. Smithson CL, Bakhshi NN. The kinetics and mechanism of the hydration of magnesium oxide in a batch reactor. Can J Chem Eng. 1969;47(6):508-13. http://dx.doi.org/10.1002/cjce.5450470602.
21. Sutcu M, Akkurt S, Okur S. A microstructural study of surface hydration on a magnesia refractory. Ceram Int. 2010;36(5):1731-5. http://dx.doi.org/10.1016/j.ceramint.2010.02.043.
22. Fruhwirth O, Herzog GW, Hollerer I, Rachetti A. Dissolution and hydration kinetics of MgO. Surf Technol. 1985;24(3):301-17. http://dx.doi.org/10.1016/0376-4583(85)90080-9.
23. Birchal VSS, Roch SDF, Ciminelli VST. Effect of magnesite calcination conditions on magnesia hydration. Miner Eng. 2000;13(14-15):1629-33. http://dx.doi.org/10.1016/S0892-6875(00)00146-1.
24. Birchal VS, Rocha SDF, Mansur MB, Ciminelli VST. A simplified mechanistic analysis of the hydration of magnesia. Can J Chem Eng. 2001;79(4):507-11. http://dx.doi.org/10.1002/cjce.5450790406.
25. Lee JH, Eun JH, Kim SG, Park SY, Lee MJ, Kim HJ. Hydration behavior of MgO single crystals and thin films. J Mater Res. 2003;18(12):2895-903. http://dx.doi.org/10.1557/JMR.2003.0404.
26. Rocha SDF, Mansur MB, Ciminelli VST. Kinetics and mechanistic analysis of caustic magnesia hydration. J Chem Technol Biotechnol. 2004;79(8):816-21. http://dx.doi.org/10.1002/jctb.1038.
27. Tang XJ, Du ZY, Zhu YM, Liu PF, Li XY, Xu XL, et al. Correlation between microstructure and dissolution property of magnesium hydroxide synthesized via magnesia hydroxylation: effect of hydration agents. J Clean Prod. 2020;249:119371. http://dx.doi.org/10.1016/j.jclepro.2019.119371.
28. Salomão R, Arruda CC, Kawamura MA. A systemic investigation on the hydroxylation behavior of caustic magnesia and magnesia sinter. Ceram Int. 2015;41(10):13998-4007. http://dx.doi.org/10.1016/j.ceramint.2015.07.012.
29. Salomão R, Arruda CC, Souza ADV, Fernandes L. Novel insights into MgO hydroxylation: effects of testing temperature, samples' volume and solid load. Ceram Int. 2014;40(Suppl 9 Part B):14809-15. http://dx.doi.org/10.1016/j.ceramint.2014.06.074.
30. Huang L, Yang Z, Wang S. Influence of calcination temperature on the structure and hydration of MgO. Constr Build Mater. 2020;262:120776. http://dx.doi.org/10.1016/j.conbuildmat.2020.120776.
31. Gao PW, Wu SX, Lin PH, Wu ZR, Tang MS. Morphology of MgO hydration products under different curing conditions. Wuji Huaxue Xuebao. 2007;23(6):1063-8.
32. Aphane ME, Van Der Merwe EM, Strydom CA. Influence of hydration time on the hydration of MgO in water and in a magnesium acetate solution. J Therm Anal Calorim. 2009;96(3):987-92. http://dx.doi.org/10.1007/s10973-008-9095-y.
33. Henrist C, Mathieu JP, Vogels C, Rulmont A, Cloots R. Morphological study of magnesium hydroxide nanoparticles precipitated in dilute aqueous solution. J Cryst Growth. 2003;249(1-2):321-30. http://dx.doi.org/10.1016/S0022-0248(02)02068-7.
34. Lv J, Qiu L, Qu B. Controlled growth of three morphological structures of magnesium hydroxide nanoparticles by wet precipitation method. J Cryst Growth. 2004;267(3-4):676-84. http://dx.doi.org/10.1016/j.jcrysgro.2004.04.034.
35. Hsu JP, Nacu A. Preparation of submicron-sized $Mg(OH)_2$ particles through precipitation. Colloidal Surfaces A. 2005;262(1-3):220-31. http://dx.doi.org/10.1016/j.colsurfa.2005.04.038.
36. Yan C, Xue D, Zou L, Yan X, Wang W. Preparation of magnesium hydroxide nanoflowers. J Cryst Growth. 2005;282:448-54. http://dx.doi.org/10.1016/j.jcrysgro.2005.05.038.
37. Wang W, Qiao X, Chen J, Li H. Facile synthesis of magnesium oxide nanoplates via chemical precipitation. Mater Lett. 2007;61(14-15):3218-20. http://dx.doi.org/10.1016/j.matlet.2006.11.071.
38. Chen D, Zhu L, Liu P, Zhang H, Xu K, Chen M. Rod-like morphological magnesium hydroxide and magnesium oxide via a wet coprecipitation process. J Porous Mater. 2009;16(1):13-8. http://dx.doi.org/10.1007/s10934-007-9162-y.

39. Liu JP, Wang YJ, Tian Q, Zhang SZ. Modeling hydration process of magnesia based on nucleation and growth theory: the isothermal calorimetry study. Thermochim Acta. 2012;550(20):27-32. http://dx.doi.org/10.1016/j.tca.2012.09.033.
40. Salomão R, Arruda CC, Antunes MLP. Synthesis, dehydroxylation and sintering of porous $Mg(OH)_2$-MgO clusters: evolution of microstructure and physical properties. InterCeram. 2020;69(1):52-62. http://dx.doi.org/10.1007/s42411-019-0067-y.
41. Khangaonkar PR, Othman R, Ranjitham M. Studies on particle breakage during hydration of calcined magnesite. Miner Eng. 1990;3(1-2):227-35. http://dx.doi.org/10.1016/0892-6875(90)90095-S.
42. Láska M, Valtýni J, Fellner P. Influence of pH on the crystal size distribution of Mg(OH)2 prepared by the hydration of MgO. Cryst Res Technol. 1993;28(7):931-6. http://dx.doi.org/10.1002/crat.2170280709.
43. Zheng L, Xuehua C, Mingshu T. Hydration and setting time of MgO-type expansive cement. Cement Concr Res. 1992;22(1):1-5. http://dx.doi.org/10.1016/0008-8846(92)90129-J.
44. Chatterji S. Mechanism of expansion of concrete due to the presence of dear-burnt CaO and MgO. Cement Concr Res. 1995;25:51-6.
45. Santos T, Santos J, Luz AP, Pagliosa C, Pandolfelli VC. Kinetic control of MgO hydration in refractory castables by using carboxylic acids. J Eur Ceram Soc. 2018;38(4):2152-63. http://dx.doi.org/10.1016/j.jeurceramsoc.2017.11.046.
46. Filippou D, Katiforis N, Papassiopi N, Adam K. On the kinetics of magnesia hydration in magnesium acetate solutions. J Chem Technol Biotechnol. 1999;74(4):322-8. http://dx.doi.org/10.1002/(SICI)1097-4660(199904)74:4<322:AID-JCTB35>3.0.CO;2-L.
47. Guo H, Xie J, Hu H, Li X, Fan T, Nan H, et al. Preparation of lamellar Mg(OH)2 with caustic calcined magnesia through apparent hydration of MgO. Ind Eng Chem Res. 2013;52(38):13661-8. http://dx.doi.org/10.1021/ie401669g.
48. Dung NT, Unluer C. Sequestration of CO_2 in reactive MgO cement-based mixes with enhanced hydration mechanisms. Constr Build Mater. 2017;143:71-82. http://dx.doi.org/10.1016/j.conbuildmat.2017.03.038.
49. Souza ADV, Salomão R. Evaluation of the porogenic behavior of aluminum hydroxide particles of different size distributions in castable high-alumina structures. J Eur Ceram Soc. 2016;36(3):885-97. http://dx.doi.org/10.1016/j.jeurceramsoc.2015.11.019.
50. Salomão R, Bittencourt LRM, Pandolfelli VC. A novel approach for magnesia hydration assessment in refractory castables. Ceram Int. 2007;33(5):803-10. http://dx.doi.org/10.1016/j.ceramint.2006.01.004.
51. Fernández AI, Chimenos JM, Segarra M, Fernández MA, Espiell F. Kinetic study of carbonation of MgO slurries. Hydrometallurgy. 1999;53(2):155-67. http://dx.doi.org/10.1016/S0304-386X(99)00039-0.
52. Dheilly RM, Bouguerra A, Beaudoin B, Tudo J, Queneudec M. Hydromagnesite development in magnesian lime mortars. Mater Sci Eng A. 1999;268(1-2):127-31. http://dx.doi.org/10.1016/S0921-5093(99)00085-4.
53. Rollason RJ, Plane JMC. A kinetic study of the reactions of MgO with H_2O, CO_2 and O_2: implications for magnesium chemistry in the mesosphere. Phys Chem Chem Phys. 2001;3(21):4733-40. http://dx.doi.org/10.1039/b105673p.
54. Botha A, Strydom CA. Preparation of a magnesium hydroxy carbonate from magnesium hydroxide. Hydrometallurgy. 2001;62(3):175-83. http://dx.doi.org/10.1016/S0304-386X(01)00197-9.
55. Choi SB, Kim NW, Lee DK, Yu H. Growth mechanism of cubic MgO granule via common ion effect. J Nanosci Nanotechnol. 2013;13(11):7577-80. http://dx.doi.org/10.1166/jnn.2013.7882.
56. Ropp RC. Encyclopedia of the alkaline earth compounds. Oxford: Elsevier; 2013. Chapter 5, Group 14 (C, Si, Ge, Sn, and Pb) alkaline earth compounds; p. 351-480. http://dx.doi.org/10.1016/B978-0-444-59550-8.00005-3.